Conformational Ensemble and Polymorphism of the All-Atom Alzheimer's Aβ 37−42 Amyloid Peptide Oligomers

ARTICLE *in* THE JOURNAL OF PHYSICAL CHEMISTRY B · APRIL 2013

Impact Factor: 3.3 · DOI: 10.1021/jp401563n · Source: PubMed

THE JOURNAL OF PHYSICAL CHEMISTRY B

Article

pubs.acs.org/JPCB

Conformational Ensemble and Polymorphism of the All-Atom Alzheimer's Aβ_{37-42} Amyloid Peptide Oligomers

Phuong H. Nguyen*,† and Philippe Derreumaux*,†,‡

†Laboratoire de Biochimie Théorique, UPR 9080, CNRS, Université Denis Diderot, Sorbonne Paris Cité, IBPC, 13 rue Pierre et Marie Curie, 75005 Paris, France

‡Institut Universitaire de France, 103 Bvd Saint-Germain, 75005 Paris, France

ABSTRACT: Although the Aβ_{37-42} peptide has two opposite terminal charges, counterintuitively its current fibril amyloid structure reveals in register parallel β-strands, as formed by the full length Aβ peptide. In this study, we carried out a replica exchange molecular dynamics simulation of 16 all-atom Aβ_{37-42} peptides in explicit water starting from randomized and dispersed chains. The extensive conformational sampling (48 replicas, 460 ns/replica) with a total simulation time of 23 μs allows us to obtain a full picture on the equilibrium conformational distribution of oligomers and β-sheet sizes and gain some insights into the oligomerization process at 300 K. At the peptide concentration of 12 mM, self-assembly is described by the condensation-polymerization mechanism with conversion from micelle-like to high β-sheet structures. At equilibrium, the oligomer distribution consists of large aggregates and free monomers, representing 70% and 25% of all species, respectively. Though the formation/dissociation of β-strand is high, the population of 4−5 fully parallel β-strands, consistent with the arrangement in the current fibril, is marginal and that of 4−5 fully antiparallel β-strands, consistent with amyloid polymorphism, is non-negligible. However, the system adopts essentially mixed parallel/antiparallel β-strands. This indicates that a system of 16 Aβ_{37-42} chains in explicit solvent still does not form more stable species that will irreversibly grow to a fibril, independently of polymorphism. Our results also suggest that the Aβ_{37-42} fibril may display packing polymorphism with antiparallel β-strands, in addition to the experimentally observed in register parallel β-strands.

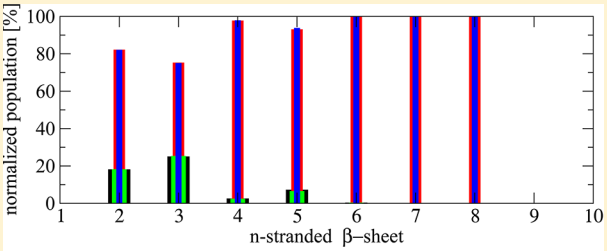

Relative normalized populations of forming n fully well-ordered parallel or antiparallel β-strands

INTRODUCTION

Protein aggregation has attracted considerable attention because of its implication in neurodegenerative diseases.[1] To this end, numerous experimental studies, including TEM, AFM, X-ray fiber diffraction,[2−4] solid-state NMR,[5−7] X-ray micro-crystallography,[8] and infrared (IR) spectroscopy,[9,10] have been performed leading to a microscopic picture of the assembly process.

These studies have confirmed that (i) amyloid fibrils adopt a cross-β structure with the β-sheets perpendicular to the fibril axis and a hydrogen bond network parallel to the fibril axis and (ii) prefibrillar oligomers are metastable undergoing many conformational fluctuations. Most importantly, oligomers are the most toxic species[1] in neurodegenerative diseases, motivating numerous experimental and theoretical studies.

Simulations of amyloid peptide aggregation represent a numerical challenge.[11,12] They require an accurate force field, and a good sampling of conformational space. Recently, we studied the influence of the GROMOS,[13] OPLS,[14] and AMBER ff94[15] force fields on the equilibrium structures of the dimer and trimer of the Alzheimer's Aβ_{16-22} fragment in explicit solvent.[16] We found that AMBER does not predict any β-sheet structure, whereas GROMOS favors antiparallel β-sheet structures, and OPLS predicts diverse structures. The impact of all-atom force fields on the stability of preformed β-sheet oligomers has also been discussed.[17,18]

Standard all-atom simulations of amyloid peptides in explicit water explore time scales of 50 - 300 ns by molecular dynamics (MD) simulations[19−21] and oligomer sizes ranging from dimers to 8-mers using MD or replica exchange molecular dynamics (REMD) simulations.[16,22−25] Recently, de Groot and co-workers followed the 10-mer aggregates formed by three peptides, VQIVYK, VEALYL, and GVATVA, using multiple all-atom MD simulations at 300 K (10 trajectories, each of 300 ns with an integration time step of 5 fs) in explicit solvent with the GROMOS force field.[26] In another work, Baftizadeh et al. studied the aggregation in explicit solvent of 18 Val8 all-atom chains employing bias-exchange metadynamics[27] with 8 different collective variables so as to explore increasing number of fully parallel or antiparallel β-sheets and steric zipper contacts. They found a transition from mixed to parallel β-strand orientation, but the population of the oligomer with fully parallel β-strands was marginal with respect to the amorphous aggregates.[28]

Received: February 13, 2013
Revised: April 12, 2013
Published: April 13, 2013

   dx.doi.org/10.1021/jp401563n | J. Phys. Chem. B 2013, 117, 5831−5840

Several coarse-grained lattice[29−32] and off-lattice models[33−50] have also been employed and provided valuable insights into the early steps of oligomerization, the role of reptation of the peptides in the late steps of aggregation, the presence of kinetic traps and unexpected topologies such as the β-barrel, the phase transition between disordered and ordered aggregates, and the connection between macroscopic observables and microscopic assembly events.

Overall, despite the number of simulations performed, we are still lacking a detailed picture of the conformational ensemble of a large number of chains for an heteropeptide at atomic level in explicit solvent. To this end, we report an all-atom REMD simulation of 16 $A\beta_{37-42}$ chains for 460 ns/replica. The amyloid fibril structure of $A\beta_{37-42}$ was determined at pH 7.5 by Eisenberg et al.,[51] revealing antiparallel β-sheets and parallel β-strands within the sheets. This feature is counterintuive since the peptide has two opposite charges at the extremities. To our best knowledge, this is the longest REMD simulation of an hexadecamer amyloid peptide in explicit aqueous solution starting from randomized and disordered chains. This extensive conformational sampling allows us to address several questions. What is the equilibrium population distribution of oligomers and β-sheets? What is the fraction of mixed parallel/antiparallel β-sheets? What is the critical nucleus size? What is the mechanism of forming ordered aggregates? And do these answers depend on the force field used and the amyloidogenic character of the peptide? Thus far this amyloid-forming fragment has been the subject of atomistic MD simulations of 25 ns at 300 K. Starting from a fibril-like structure with two antiparallel β-sheets, each sheet composed of 8 parallel β-strands, Thirumalai et al. examined the molecular events that occur as the two sheets initially solvated approach each other.[52]

MATERIAL AND METHODS

Simulation Details. The simulated sequence is Gly-Gly-Val-Val-Ile-Ala, i.e., free of Ace and NH2 capped ends, but with both termini charged oppositely as used experimentally for fibril formation. We used the TIP3P[53] water model with the CHARMM27 force field.[54] The initial configuration of the monomer $A\beta_{37-42}$ was extracted from the structure of the $A\beta_{17-42}$ peptide available in the Protein Data Bank (ID: 2BEG).[7] The initial configuration of the 16-mer was obtained by replicating the monomer structure in randomized orientations and positions in a periodic cubic box containing 6700 water molecules, leading to a peptide concentration of 12 mM. The system was then minimized using the steepest descent method and equilibrated for 1 ns at constant pressure (1 atm) and temperature (T = 300 K), respectively, using the Berendsen coupling method.[55] The system was subsequently equilibrated at constant temperature (T = 300 K) and constant volume for 1 ns, and the resulting structure consisting of randomized and fully dispersed monomeric chains was used for all replicas in the REMD simulation.

The GROMACS program suite[56] was employed. The equations of motion were integrated by using a leapfrog algorithm with a time step of 2 fs. Covalent bond lengths were constrained via the SHAKE[57] procedure with a relative geometric tolerance of 10^{-4}. We used the particle-mesh Ewald method to treat the long-range electrostatic interactions.[58] The nonbonded interaction pair-list was updated every 5 fs, using a cutoff of 1.2 nm. The Berendsen coupling method[55] was used to couple each system to the heat bath with a relaxation time of 0.1 ps.

Given the lowest (290 K) and highest (410 K) temperatures and requesting an acceptance ratio of ∼20%, the temperatures of the replicas were determined by using the method recently proposed by Patriksson and van der Spoel.[59,60] This resulted in 48 replicas. Exchanges between replicas were attempted every 1.5 ps, large enough compared to the coupling time of the heat bath. Each replica was run for 460 ns and the data were collected every 2 ps.

Data Analysis. To characterize the structures and the assembly process, we used several properties including secondary structures, order parameters, oligomer sizes, β-sheet sizes and their orientations, free energy landscape and 3D structures.

Secondary Structures. We monitored the secondary structure composition of the system using the "broad" definition as reported in ref.[61] Following this definition, if backbone dihedral angles (ϕ,ψ) are discretized into 20 intervals of 18°, then a β state corresponds to the vertices of the polygon (−180,180), (−180,126), (−162,126), (−162,108), (−144,108), (−144,90), (−50,90), (−50,180) on the Ramachandran plot, and the α helix state is confined to the polygon (−90,0), (−90,-54), (−72,-54), (−72,-72), (−36,-72), (−36,-18), (−54,-18), (−54,0), all other regions are considered as coil. The peptide is in the β (α helix) conformation if (i) the (ϕ,ψ) angles of any two consecutive residues are in the corresponding β (α helix) states and (ii) no two consecutive residues are in α helix (β) states. If neither β nor α helix conformations are assigned, then the peptide is classified as random coil. Our results obtained using this definition are very similar to that used by STRIDE.[62]

Order Parameter. Let $\vec{u}_i = \{u_{\alpha i}\}$, ($\alpha$ = x,y,z) be the unit vector of the end-to-end distance that connects the C_α atom termini of the ith peptide. Let $\mathbf{Q}$ be the orientational tensor,[63] whose components have the form

$$Q_{\alpha\beta} = \frac{1}{N}\sum_{i=1}^{N}(u_{\alpha i}u_{\beta i}) - \frac{1}{3}\delta_{\alpha\beta} \quad (1)$$

where N is the number of peptides and $\delta_{\alpha\beta}$ is the Kronecker's symbol. This expression (eq 1) defines the components of a symmetric tensor rank two with zero trace, which generally has five independent components. Such a tensor can be diagonalized and as a result, it is possible to find the eigenvectors $\mathbf{n}_1$, $\mathbf{n}_2$, and $\mathbf{n}_3$ and the eigenvalues λ_1, λ_2, and λ_3. The maximum eigenvalue λ_{max} determines the order parameter P_2

$$P_2 = \frac{3}{2}\langle\lambda_{max}\rangle \quad (2)$$

while the director corresponds to the unit vector $\mathbf{n}$ whose characteristic value is λ_{max}. We define that the system has the propensity to form fibril-like conformation if P_2 is >0.5.[64]

Oligomer Size. The oligomer size, $N_{oligomer}$, was defined as the number of peptides which are consecutively in contact. A contact was considered formed if the shortest distance between the centers of mass of two residues belonging to two chains is less than 0.65 nm.

β-Sheet Size. The β-sheet size, $N_{\beta-sheet}$, is the number of peptides which are consecutively connected by at least two backbone hydrogen bonds with all chains adopting the β structure. A hydrogen bond (H-bond) is formed if the distance between the N and O atoms is less than 0.35 nm and the angle (CON) is greater than 120°.

dx.doi.org/10.1021/jp401563n | J. Phys. Chem. B 2013, 117, 5831−5840

Pairs of Two Parallel (P) or Antiparallel (AP) β-Strands. For a given β-sheet size, it is instructive to count the number of pairs of two consecutive P (AP) well-ordered β-strands since the formation of mixed P/AP β-strands is an expected configuration. Here one pair of two P (AP) β-strands is a configuration with both chains adopting the β structure, forming at least two backbone H-bonds and having the cosine angle between their end-to-end vectors using all residues greater than 0.5 (less than −0.5).

Relative Orientation of Two β-Sheets. To characterize the relative orientation between two β-sheets, it is convenient to work in a molecular fixed frame, in which the *z*-axis points along the vector connecting the centers of mass of two sheets (Figure 1). We constructed three eigenvectors $\mathbf{n}_1$, $\mathbf{n}_2$, and $\mathbf{n}_3$ from the orientational tensor of only monomers within the β-sheet. The vectors $\mathbf{n}_1$ associated with the largest eigenvalue is almost parallel to the β-strand direction, $\mathbf{n}_2$ associated with the second largest eigenvalue is almost parallel to the main chain hydrogen bonding direction and $\mathbf{n}_3$ associated with the smallest eigenvalue is almost perpendicular to the β-sheet. The relative orientation between two β-sheets is described by four angles (θ_1,ϕ_1) and (θ_2,ϕ_2) which specify the orientations of two director vectors $\mathbf{n}_1$ and $\mathbf{n}_2$ associated to two sheets, respectively, in the molecular fixed frame.

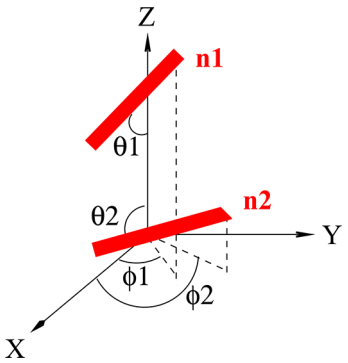

Figure 1. Molecular fixed-frame used to describe the relative orientation between two β-sheets. The *z*-axis points along the vector connecting the centers of mass of two sheets. The orientation of a sheet is characterized by two angles (θ,ϕ) which describe the orientation of the director vectors **n** (red).

Free Energy Landscape. To characterize the aggregates, we employed two reaction coordinates, namely the total number of interpeptide backbone hydrogen bonds, Hb, within the β-sheets and the average distance *d* between the centers of mass of two β-sheets, which reflect, respectively, the longitudinal elongation of the β-sheets in the main chain hydrogen bonding direction and the lateral growth of β-sheets. The free energy landscape is given by $G(Hb,d) = -k_BT[\ln P(Hb,d) - \ln P_{max}]$, where $P(Hb,d)$ is the probability distribution obtained from a histogram of the data and P_{max} is the maximum of the distribution, which is subtracted to ensure that $G = 0$ for the lowest free energy minimum.

RESULTS

In what follows, we combine the data from the trajectories at 300 and 302 K to increase the statistics of the analysis, and exclude the first 100 ns of each replica for equilibration, unless stated explicitly. Convergence of the simulation was assessed by comparing properties using 100−400 and 100−460 ns.

Overall Picture of the Oligomerization Process. To obtain a first picture on the oligomerization process, Figure 2 shows the time evolution of four global reaction coordinates using the full 460 ns at 300 K and the resulting distributions using 100−460 ns. Following the time evolution of secondary structure, we see an increase in the β content from 25% to 75%,

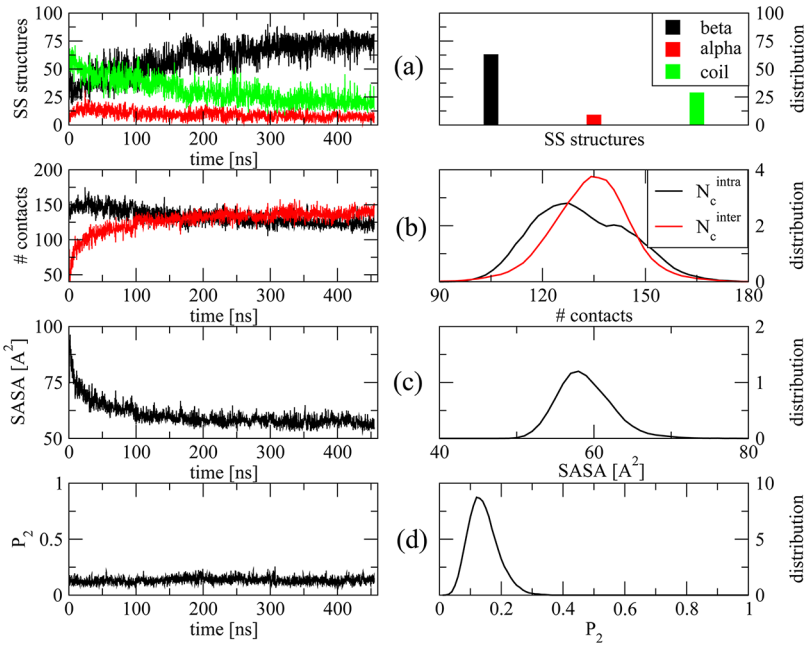

Figure 2. Time evolution (left panels) and equilibrium distribution (right panel) of four global variables: the secondary structure composition (a), the total number of intrapeptide (N_c^{intra}) and interpeptide (N_c^{inter}) side-chain side-chain contacts (b), the total solvent accessible surface area SASA (c), and the order parameter P_2 (d). Shown are results of the time evolution at 300 K using the 460 ns and of the distributions at 300 and 302 K using 100−460 ns.

dx.doi.org/10.1021/jp401563n | J. Phys. Chem. B 2013, 117, 5831−5840

whereas the α and coil contents decrease from 20 and 50% to 10 and 25%, respectively. This is accompanied by the decrease in the total number of intrapeptide contacts N_c^{intra} from 160 to 125, and an increase in the interpeptide contacts N_c^{inter} from 50 to 140. During peptide oligomerization, waters are expelled and the peptides become drier as reflected by the decrease of the total peptide solvent accessible surface area, SASA, from 90 to 60 Å^2. Surprisingly, the order parameter P_2 varies little and remains small during the whole simulation. Single exponential fits of the time evolution for the β content and the solvent accessible surface area lead to time scales of 190 and 28 ns, respectively. As expected, the initial stage of the assembly process is driven by a hydrophobic collapse, and the late events involve change in secondary and tertiary structures.

As seen from Figure 2, the distributions of the four global coordinates are basically Gaussians indicating that they are not able to capture any intermediates within 100−460 ns. Averaged over all conformations, the system is characterized by 70, 10, and 30% of β-strand, α-helix, and random coil, respectively. There are about 120 and 135 intra- and interpeptide contacts, respectively, and the total solvent accessible surface area is about 40 Å. The average value of the P_2 parameter is about 0.15, much lower than the threshold of 0.5, indicating therefore the absence of fibril-like configuration at least for the full system. The distributions do not change at all using 100−400 ns (data not shown).

Equilibrium Distribution of Oligomers and β-Sheets. First, we wish to obtain a detailed picture on the equilibrium population distribution of the oligomers and β-sheets within 100 - 460 ns. To this end, we define the relative normalized population of an oligomer or a β-sheet of size n as $P_{oligomer/\beta-sheet}(n) = 100 \times \langle N_{oligomer/\beta-sheet}(n,t)\rangle / \sum_n \langle N_{oligomer/\beta-sheet}(n,t)\rangle$, where $N_{oligomer/\beta-sheet}(n,t)$ is the number of oligomers or β-sheets composed of n peptides at time t, and $\langle\cdots\rangle$ denotes time average. Convergence was checked by using 100−400 and 100−460 ns and the results are essentially identical. As shown in Figure 3, at the concentration of 12 mM, the system consists of 16-mers and 15-mers with relative populations of ∼50 and 17%, respectively, in equilibrium with free monomers (population of 25%). This high fraction of free monomers indicates the plasticity of the system and that the association/dissociation process always takes place. There is also a small population of 2-mers, 13-mers, and 14-mers, totalling 7%.

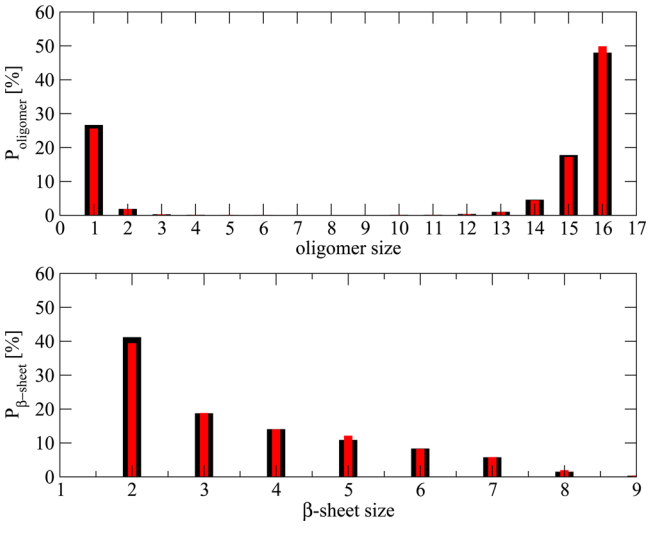

Figure 3. Relative normalized population distributions of oligomers (upper panel) and β-sheets (lower panel). Shown are results at 300 and 302 K using the 100−400 ns (black) and 100−460 ns (red) time windows.

For the β-sheet distribution, Figure 3, we observe a decay of the relative population as the size increases. The 2-stranded β-sheet is dominant with a normalized relative population of 40% compared to the values of 18, 14, 12, 8, and 6% for the 3-stranded, 4-stranded, 5-stranded, 6-stranded, and 7-stranded β-sheets, respectively. The β-sheets composed of 8 chains form with relative populations of 2%, and 9- and 10-stranded β-sheets are also observed, but with negligible populations.

Next, we wish to obtain a spatial-orientational picture of the β-sheet arrangement. To this end, we calculated the distances between the centers of mass of any two sheets and the distribution is shown in Figure 4. As seen, the distribution displays two well-defined peaks at short distances and a third peak of lowest intensity at $r \approx 3$ nm. To further characterize the orientational order of the sheets belonging to each peak, we calculated the joint probability distribution of the angles $P(\theta_1,\theta_2)$ and $P(\phi_1,\phi_2)$. The first peak, P1, corresponding to the shortest distance between two sheets, is located at $r \approx 1-1.2$ nm. The distribution $P_1(\theta_1,\theta_2)$ shows a high probability located at ($\theta_1 \approx 90°$, $\theta_2 \approx 90°$) and ($\theta_1 \approx 60°$, $\theta_2 \approx 60°$) indicating that two sheets are essentially parallel or antiparallel. Furthermore, the distribution $P_1(\phi_1,\phi_2)$ also shows a high probability at ($\phi_1 \approx 180°$, $\phi_2 \approx 180°$) indicating that the β-strands within two β-sheets are also essentially parallel or antiparallel. The second peak P2, located at $r \approx 2$ nm, is found to be associated with two second nearest neighbor β-sheets. The distributions $P_2(\theta_1,\theta_2)$ and $P_2(\phi_1,\phi_2)$ are centered around ($\theta_1 \approx 60°$, $\theta_2 \approx 60°$) and ($\phi_1 \approx 180°$, $\phi_2 \approx 180°$), respectively. In contrast, the third peak, P3 at $r \approx 3$ nm, corresponding to the third nearest neighbor β-sheets, does not show very well-ordered orientation as indicated by the scattered distributions of the θ and ϕ angles. Overall, our system consists essentially of two β-sheet layers separated by a distance very similar to that observed in the Aβ_{37-42} amyloid fibril structure,[51] and three β-sheet layers randomly packed.

Parallel/Antiparallel β-Sheets. Given a β-sheet composed of n β-strands, we want to determine (i) the relative normalized probabilities of forming n fully well-ordered parallel or antiparallel β-strands and (ii) the relative normalized populations of pairs of two parallel or two antiparallel β-strands within that sheet. The results displayed in Figure 5 show that fully antiparallel β-strands are favored over fully parallel β-strands independently of the β-sheet size. When n-stranded β-sheets form, the relative populations of two, three, four and five parallel β-strands are 18, 23, 2, and 4% and their occurrence probabilities in all configurations within 100−460 ns are 15%, 5%, < 1% and <2%. In contrast, we find the occurrence probabilities of forming n-stranded fully antiparallel β-sheets vary from 47% (n = 2), 9% (n = 3), 8% (n = 4), 3% (n = 5), and 1% (n = 6) to much less than 1% for n = 7 and 8. Again, extending the analysis from 400 to 460 ns does not change the statistics.

The relative normalized populations of pairs of parallel (∼20%) and antiparallel (∼80%) β-strands within a given β-sheet do not depend significantly on the β-sheet size (Figure 5). This indicates both pairs of parallel and antiparallel chains form during the elongation of β-sheets. Finally, looking at the mixed parallel/antiparallel (P/AP) strands when β-sheets form, we

dx.doi.org/10.1021/jp401563n | J. Phys. Chem. B 2013, 117, 5831−5840

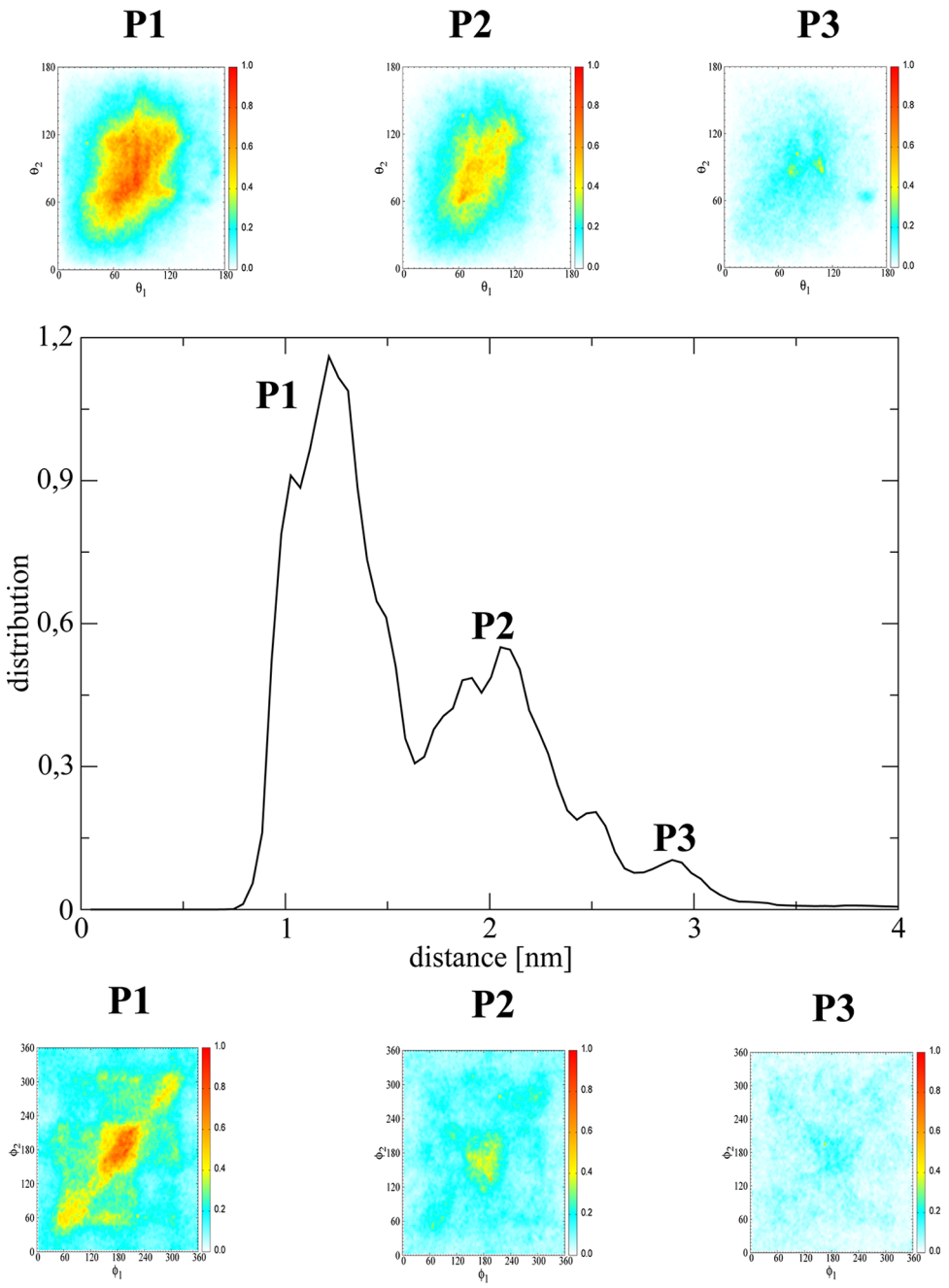

Figure 4. Spatial-orientational characterization of β-sheets using the trajectories at 300 and 302 K within 100−460 ns. Shown is the population distribution of the distance between the centers of mass of any two β-sheets (middle). For each peak P_i (i = 1, 2, 3) on this distribution, the probability distributions of the angles $P_i(\theta_1,\theta_2)$ and $P_i(\phi_1,\phi_2)$ are also shown. The color gradient from white to red indicates an increase in probability.

find that they are more populated than fully P or fully AP strands and their probabilities increase with the β-sheet size, varying from 55% (3-stranded), 49% (4-stranded), 73% (5-stranded), to more than 90% (6, 7, 8, and 9-stranded).

Insights into the Formation Process of Ordered Aggregates. Although the REMD trajectory does not allow us to follow oligomerization in time, information on the conversion from compact disordered to ordered aggregates within 100 - 460 ns can be extracted by determining how a pair of parallel β-strands or antiparallel β-strands is formed. To form a pair of parallel or antiparallel β-strands at time step t + 1, each of two peptides at the previous time step can be (1) random coil or α helix (strand−strand association), (2) one is random coil or α helix and the other is within a β-sheet (strand−β-sheet association), and (3) both peptides are within two separated β-sheets (β-sheet−β-sheet association or condensation). To identify the dominant process, we calculated the total number of association events between two peptides i and j within the time interval (t,t + 1) for the three mechanisms k (k = 1,2,3): $N^k_{\text{para/antipara}}(t) = \sum_{i,j=i+1}^{Np} C^k_{ij}$, where C^k_{ij} = 0 if peptides i,j do not form a pair of parallel/antiparallel β-strands at time t, C^k_{ij} = 1 if peptides i,j do form a pair of parallel/antiparallel β-strands at time t + 1, and Np is the total number of peptides involved in each association process. To compare the association mechanisms, we also calculated their frequencies and results are displayed in Figure 6. Interestingly, the frequency of each

dx.doi.org/10.1021/jp401563n | J. Phys. Chem. B 2013, 117, 5831−5840

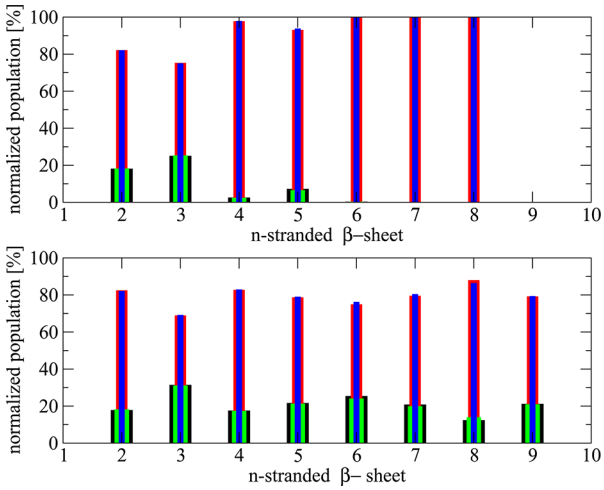

Figure 5. (Upper panel) Relative normalized populations of forming n fully well-ordered parallel (black, green) or antiparallel (red, blue) β-strands. (Lower panel) Relative normalized population of the pairs of two parallel (black, green) or antiparallel β-strands (red, blue) within a n-stranded β-sheet. Shown are results at 300 and 302 K, using the 100–400 ns (black, red) and 100–460 ns (green, blue) time windows.

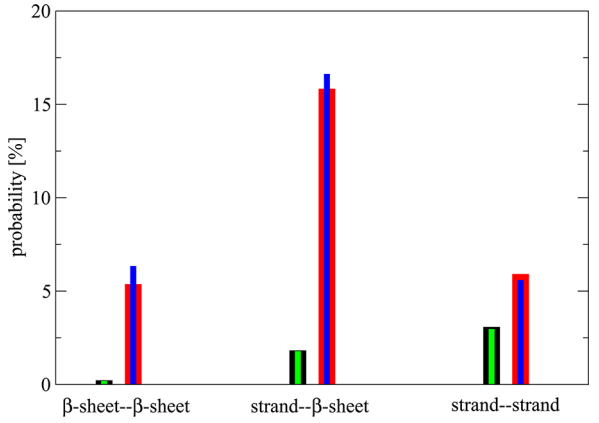

Figure 6. Probability of forming pairs of two parallel (black, green) or antiparallel (red, blue) β-strands due to the β-sheet–β-sheet, strand–β-sheet, and strand–strand associations using the 100–400 ns (black, red) and 100–460 ns (green, blue) time windows at 300 and 302 K.

mechanism vary from parallel to antiparallel association. For the parallel case, the strand–strand and strand–β-sheet associations occur 3% of the time and the frequency of β-sheet–β-sheet association is very small. For the antiparallel case, the probability for strand–β-sheet association is rather high (16% of the time), and the occurrence probabilities for strand–strand and β-sheet–β-sheet association amount to 6%. Note we find the same occurrence probabilities for the three dissociation mechanisms using the same procedure.

Information on the aggregation can also be extracted from the free energy landscape using the full REMD trajectories at 300 and 302 K projected on two reaction coordinates: the number of interpeptide backbone hydrogen bonds within β-sheets and the averaged distance between the centers of mass of β-sheets. Figure 7 shows the resulting free energy landscape. At T = 300 and 302 K there are nine close-lying local minima denoted as Si (i = 1, ..., 9). A representative structure of each minimum is also shown. We note that these minima are separated by low free energy barriers ~1 kcal/mol. Table Table

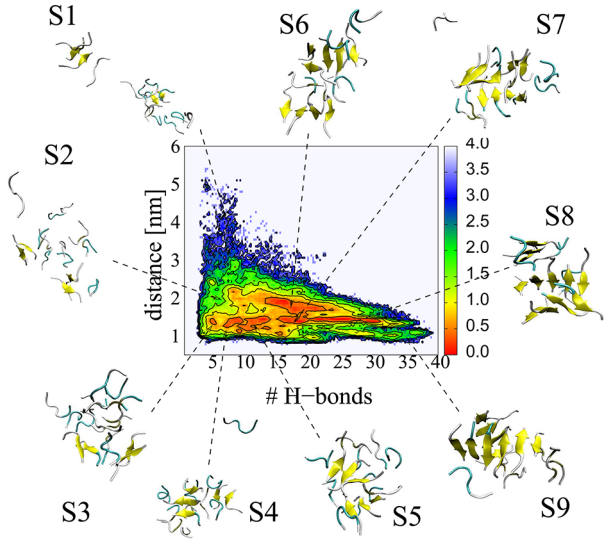

Figure 7. Free energy landscape of the hexadecamer using the full REMD trajectory at 300 and 302 K. Shown are results along the number of hydrogen bonds within β-sheets and the mean distance between the centers of mass of β-sheets. The centers of each cluster corresponding to the main minima are shown with the β-strands in yellow. The color gradient from red to blue shows the increase in free energy (kcal/mol).

1 shows, for each state, the population, the mean number of β-sheets $\langle N_{\text{sheet}}\rangle$, the mean number of β-strands in β-sheets $\langle N_{\text{strand}}\rangle$, the mean number of interpeptide backbone hydrogen bonds within β-sheets $\langle N_{\text{Hb}}\rangle$, the mean distance between the centers of mass of β-sheets $\langle N_{\text{com}}\rangle$, and the mean angles $\langle\theta_i\rangle$, $\langle\phi_i\rangle$ together with their standard deviations $\delta\theta_i$, $\delta\phi_i$ (i = 1,2). On average, the state S1 (2%) has two β-sheets separated by a distance of 3.5 nm, each composed of two β-strands with five interpeptide backbone hydrogen bonds. The states S2 (2%) and S3 (8%) have also two β-sheets composed of two β-strands, but they are much closer in space ($\langle d_{\text{com}}\rangle$ = 2.46 and 1.33 nm, respectively). The states S4 (12%) and S5 (14%) also have two β-sheets, separated by short distances ($\langle d_{\text{com}}\rangle$ = 1.33 and 1.32 nm, respectively), but they are of larger size ($\langle N_{\text{strand}}\rangle$ = 5 and 6, respectively), reflecting the initial elongation of sheets. The minima S6 (16%) and S7 (12%) show a growth of layers (2.8 and 2.5 β-sheets) and an extension of the β-strands (9 chains on average). These simultaneous longitudinal and equatorial mechanisms lead to more ordered β-sheet oligomers: S8 (19%) and S9 (6%) with 12 and 14 β-strands, two and three β-sheets, and 26 and 33 hydrogen bonds between the strands, respectively.

The "diagonal" shape of the free energy landscape allows us to draw an overall picture on the formation of transient ordered β-rich aggregates. In the first stage, polymerization driven by a hydrophobic collapse takes place resulting in various oligomer sizes with little and small β-strands (S1, S2, and S3). Then, within the amorphous aggregates, two small β-sheets extend by monomer addition (S4 and S5) and further conversion of peptides from random coil to β-strand conformations can either lead to larger β-sheets (S6, S7, and S9) or the formation of a new β-sheet layer (S8).

DISCUSSION AND CONCLUSIONS

We performed an unbiased REMD simulation to study the aggregation process of 16 Aβ_{37-42} chains using the all-atom

dx.doi.org/10.1021/jp401563n | J. Phys. Chem. B 2013, 117, 5831–5840

Table 1. Characterization of the Conformational States (S) Indicated on the Free Energy Landscape Shown in Figure 7[a]

S	P [%]	$\langle N_{sheet}\rangle$	$\langle N_{strand}\rangle$	$\langle N_{Hb}\rangle$	$\langle d_{com}\rangle$	$\langle\theta_1\rangle \pm \delta\theta_1$	$\langle\theta_2\rangle \pm \delta\theta_2$	$\langle\phi_1\rangle \pm \delta\phi_1$	$\langle\phi_2\rangle \pm \delta\phi_2$
1	2	2.0	4	5	3.51	71 ± 35	90 ± 40	197 ± 85	157 ± 94
2	2	2.0	4	5	2.46	70 ± 36	79 ± 43	191 ± 82	194 ± 98
3	8	2.0	4	6	1.33	71 ± 35	83 ± 39	184 ± 95	175 ± 102
4	12	2.0	5	7	1.33	75 ± 35	84 ± 37	178 ± 91	174 ± 96
5	14	2.1	6	10	1.32	79 ± 33	87 ± 37	174 ± 86	178 ± 93
6	16	2.8	9	17	1.82	77 ± 29	83 ± 34	183 ± 81	182 ± 83
7	12	2.5	9	17	1.27	86 ± 29	100 ± 31	176 ± 81	175 ± 82
8	19	3.3	12	26	1.49	79 ± 26	82 ± 28	175 ± 69	176 ± 72
9	6	2.5	14	33	1.25	72 ± 26	74 ± 27	171 ± 67	175 ± 73

[a]Shown are the population P (in %), the mean values of the number of β-sheets $\langle N_{sheet}\rangle$, the number of β-strands within β-sheets $\langle N_{strand}\rangle$, the number of interpeptide backbone hydrogen bonds within β-sheets $\langle N_{Hbond}\rangle$, the centers of mass distance (in nm) between β-sheets $\langle d_{com}\rangle$, and the orientational angles (in degree) of β-sheets ($\langle\theta_i\rangle$, $\langle\phi_i\rangle$), together with their standard deviations ($\delta\theta_i$,$\delta\phi_i$) (i = 1,2).

CHARMM force field and TIP3P water model. We used a peptide concentration of 12 mM similar to prior simulations[19,26] to accelerate the assembly process, the protein concentration examined in vitro varying from 10 μM to 20 mM. The extensive conformational sampling (48 replicas, 460 ns/replica) allows us to determine the equilibrium structures and investigate the formation of ordered assemblies from a disordered aggregate without any bias. Our results can be compared with recent simulations using several approaches and force fields and summarized as follows.

First, we observe that the first step of self-assembly involves a hydrophobic collapse from a random configuration to densely packed oligomers without any preferred secondary structures. In the second step, internal reorganization of the peptide starts and we observe conformational conversions from random and compact assemblies to highly β-sheet oligomers. This biphasic aggregation process is consistent with the "condensation-polymerization" mechanism observed experimentally[65] and computationally using all-atom simulations of the tau VQIVYK, insulin VEALYL and α-synuclein GVATVA fragments in explicit solvent[19] and the Aβ_{16-22} and Aβ_{25-35} fragments in implicit solvent,[66] and coarse grained MD simulations of the NNQQ and hIAPP(20−29) peptides.[40,67] Using the number of interpeptide hydrogen bonds within β-sheets and the mean distance between the centers of mass of β-sheets, the free energy landscape indicates that starting from two 2-stranded β-sheets as templates within amorphous aggregates, the assembly process follows a simultaneous elongation (longitudinal) and growth (lateral) of β-sheets. This is consistent with previous coarse-grained simulations.[35,68,69] The system is highly dynamic and heterogeneous, however, and at equilibrium the system at 300 K consists of large aggregates (16-mers, 15-mers, and 14-mers representing 70% of all conformations), small aggregates (2-mers and 3-mers representing 3%) and free monomers with a population of 25%.

Second, the global free energy minimum consists of amorphous aggregates characterized by two small β-sheets, each of 2 or 3 strands with a variety of sheet-to-sheet pairing angles surrounded by random coil peptides (S3, S4, and S5 states in Figure.7). This is consistent with bias-exchange metadynamics simulations of 18 Val8 chains in explicit water.[28] We observe, however, a non-negligible population of aggregates with 5- and 6-stranded β-sheets and find that the occurrence probabilities of forming n-stranded fully antiparallel (AP) β-sheets vary from 47% (n = 2), 9% (n = 3), 8% (n = 4), 3% (n = 5), 1% (n = 6), to much less than 1% for n = 7 and 8. In contrast, the occurrence probabilities of forming n-stranded parallel (P) β-sheets are much smaller varying from 15% (n = 2), 5% (n = 3), to less than 1 and 2% (for n = 4 and n = 5). These results indicate that the presence of two opposite charges at the extremities is not sufficient to promote strongly the formation of 5−8 fully antiparallel chains, in contrast to what has been reported for oligomers of the KFFE peptide,[70] and the conformational ensemble is still far away from the current fibril structure with parallel β-strands.[51]

We observe a high population of mixed AP/P β-sheet oligomers. This picture has also been captured using short all-atom MD simulations in explicit solvent,[19] all-atom Monte Carlo in implicit solvent[41,66] all-atom bias-exchange metadynamics in explicit solvent,[28] coarse-grained REMD, MD[71] and DMD[72] simulations. We conclude that the mixed AP/P β-sheet character of early formed oligomers is independent of the force field and molecular representation used, and is therefore a generic property of amyloid peptide self-assembly. We emphasize that only the revised coarse-grained PRIME force field coupled to DMD simulations generated fibrils with fully parallel β-strands for the tau VQIVYL fragment.[73] Whether the same force field can generate fully antiparallel β-strands for the Aβ_{16-22} and KFFE amyloid fibrils remains to be determined.

In contrast, the ratio of fully AP to fully P β-strands in early formed oligomers is impacted by the sequence composition in short peptides. For instance, the simulations of the human islet amyloid fragment NFGAIL[74] observed equal tendency to form fully parallel and antiparallel β-strands, the simulations of the yeast prion Sup-35 fragment GNNQQNY[67] and the tau fragment VQIVYK[41] showed a higher preference for fully P than fully AP β-strands, while the simulations of the insulin fragment VEALYL[26] and the fragment NNQQ[71] showed a stronger preference for fully antiparallel β-strands in oligomers.

Third, our simulations investigate the frequency of the strand−strand, strand−β-sheet, and β-sheet−β-sheet association/dissociation events. We show that the occurrence probabilities of each mechanism vary from parallel to antiparallel configurations, and the strand−β-sheet association/dissociation with antiparallel character is the most dominant event. This implies that the condensation and polymerization of β-sheets both strongly favor antiparallel associations in early formed oligomers, again at variance with the arrangement observed in the current fibril structure.[51]

Finally, our simulations provide insights into the critical nucleus size from which rapid growth of the fibril occurs.[75−77] In prior studies, the size of the critical nucleus was determined from the dependence of the free energy on the number of monomers using coarse-grained[67] or all-atom[78] simulations, the

dx.doi.org/10.1021/jp401563n | J. Phys. Chem. B 2013, 117, 5831−5840

stability of β-sheet oligomers of different sizes by all-atom MD,[79] the free energy per chain as a function of three reactions coordinates using bias-exchange metadynamics,[28] or the number of forming template peptides above which the time to add a new monomer with fibril properties is independent of the template size using on-lattice Monte Carlo simulations.[80] The nucleus size or critical β-domain size with a probability of 50% to form a fibril was also estimated by following the aggregation of a two-state peptide by Langevin dynamics.[77] Importantly, although amyloid formation is a generic property of many peptides, the nucleus size is expected to vary with the amyloidogenic character of the peptide. Using a simple two-state model, it was found that the nucleus size can vary from 4 to 35 chains.[77]

In our unbiased all-atom REMD simulation, despite we observe frequent strand−strand and strand−β-sheet formation/fragmentation events, and there is a significant reservoir of free monomers and dimers, the occurrence probability of 4−5 fully parallel β-strands, consistent with the arrangement in the current fibril structure,[51] is marginal and that of 4−5 fully antiparallel β-strands, consistent with amyloid polymorphism, is non-negligible. Looking at higher free energy minima, the aggregates consist of mixed P/AP β-strands, with few parallel β-strands surrounded by antiparallel β-strands, and vice versa. The latter feature has been already described by dynamical Monte Carlo simulations of a very simple model[44] and bias-exchange metadynamics of an heteropeptide.[28] Overall, our results indicate that the free energy of larger n-stranded fully parallel or antiparallel β-sheet is significantly higher than those of the aggregates explored here, and the critical nucleus size for the Aβ_{37-42} peptide is larger than 4−5 and 5−8 chains as reported for the GNNQQNY[67] and STVIYE[78] peptides, respectively. Whether the critical nucleus is on the order of 11−14 chains as reported on two other peptides[28,80] cannot be determined here due to finite-size effects, but also the polymporphic nature of fibrils.

Indeed, it has been observed numerically on a peptide model[77] and experimentally on the D23N-Aβ_{1-40} peptide under conditions of repeated seeding[81] that polymorphism is under kinetic control. Interestingly the peptide Aβ_{35-42}, with addition of MV amino acids, displays fibril packing polymorphism, with either parallel or antiparallel β-strands within the sheets,[82] while this type of polymorphism has not been reported thus far experimentally for Aβ_{37-42}. This is rather surprising considering the fact that the Aβ34−42 fibril also forms antiparallel β-strands in vitro.[83] We are currently exploring all these issues on a larger Aβ37−42 oligomer using atomistic and coarse-grained simulations.

AUTHOR INFORMATION

Corresponding Author

*E-mail: phuong.nguyen@ibpc.fr; philippe.derreumaux@ibpc.fr.

Notes

The authors declare no competing financial interest.

ACKNOWLEDGMENTS

This work was supported by the CNRS, the Institut Universitaire de France, and the Frankfurt Center for Scientific Computing.

REFERENCES

(1) Chiti, F.; Dobson, C. M. Protein Misfolding, Functional Amyloid, and Human Disease. *Annu. Rev. Biochem.* **2006**, *75*, 333−366.
(2) Serpell, L. C.; Sunde, M.; Benson, M. D.; Tennent, G. A.; Pepys, M. B.; Fraser, P. E. The Protofilament Substructure of Amyloid Fibrils. *J. Mol. Biol.* **2000**, *300*, 1033−1039.
(3) Sunde, M.; Blake, C. The Structure of Amyloid Fibrils by Electron Microscopy and X-ray Diffraction. *Adv. Protein Chem.* **1997**, *50*, 123−159.
(4) Harper, D. J.; Lieber, C. M.; Lansbury, P. T. J. Atomic Force Microscopic Imaging of Seeded Fibril Formation and Fibril Branching by the Alzheimer's Disease amyloid-beta protein. *Chem. Biol.* **1997**, *4*, 951−959.
(5) Petkova, A. T.; Ishii, Y.; Balbach, J. J.; Antzutkin, O. N.; Leapman, R. D.; Delaglio, F.; Tycko, R. A Structural Model for Alzheimer's beta -amyloid Fibrils Based on Experimental Constraints from Solid State NMR. *Proc. Natl. Acad. Sci. U.S.A.* **2002**, *99*, 16742−16747.
(6) Antzutkin, O. N.; Balbach, J. J.; Leapman, R. D.; Rizzo, N. W.; Reed, J.; Tycko, R. Multiple Quantum Solid-state NMR Indicates a Parallel, not Antiparallel, Organization of β -sheets in Alzheimer's beta -amyloid Fibrils. *Proc. Natl. Acad. Sci. U.S.A.* **2000**, *97*, 13045−13050.
(7) Luhrs, T.; Ritter, C.; Adrian, M.; Riek-Loher, D.; Bohrmann, B.; H, D.; Schubert, D.; Riek, R. 3D Structure of Alzheimer's Amyloid-β(1−42) Fibrils. *Proc. Natl. Acad. Sci. U.S.A.* **2005**, *102*, 17342−17347.
(8) Nelson, R.; Sawaya, M. R.; Balbirnie, M.; Madsen, A.; Riekel, C.; Grothe, R.; Eisenberg, D. Structure of the Cross-beta Spine of Amyloid-like Fibrils. *Nature* **2005**, *435*, 773−778.
(9) Petty, S. A.; Decatur, S. M. Intersheet Rearrangement of Polypeptides During Nucleation of β-sheet Aggregates. *Proc. Natl. Acad. Sci. U.S.A.* **2005**, *102*, 14272−14277.
(10) Shim, S. H.; Strasfeld, D. B.; Ling, Y. L.; Zanni, M. T. Multidimensional Ultrafast Spectroscopy Special Feature: Automated 2D IR Spectroscopy Using a mid-IR Pulse Shaper and Application of this Technology to the Human Islet Amyloid Polypeptide. *Proc. Natl. Acad. Sci. U.S.A.* **2007**, *104*, 14197−14202.
(11) Straub, J. E.; Thirumalai, D. Principles Governing Oligomer Formation in Amyloidogenic Peptides. *Curr. Opin. Struct. Biol.* **2010**, *20*, 1−9.
(12) Ma, B.; Nussinov, R. Simulations as Analytical Tools to Understand Protein Aggregation and Predict Amyloid Conformation. *Curr. Opin. Chem. Biol.* **2006**, *10*, 445−452.
(13) van Gunsteren, W.; Billeter, S. R.; Eising, A. A.; Hünenberger, P. H.; Krüger, P.; Mark, A. E.; Scott, W.; Tironi, I. *Biomolecular Simulation: The GROMOS96 Manual and User Guide*; Vdf Hochschulverlag AG an der ETH: Zurich, 1996.
(14) Kaminski, G. A.; Friesner, R. A.; Tirado-Rives, J.; Jorgensen, W. L. Evaluation and Reparametrization of the OPLS-AA Force Field for Proteins Via Comparison with Accurate Quantum Chemical Calculations on Peptides. *J. Phys. Chem. B* **2001**, *105*, 6474−6487.
(15) Wang, J.; Cieplak, P.; Kollman, P. How Well Does a Restrained Electrostatic Potential (RESP) Model Perform in Calculating Conformational Energies of Organic and Biological Molecules? *J. Comput. Chem.* **2000**, *21*, 1049−1074.
(16) Nguyen, P. H.; Li, M. S.; Derreumaux, P. Effects of All-atom Force Fields on Amyloid Oligomerization: Replica Exchange Molecular Dynamics Simulations of the Aβ_{16-22} Dimer and Trimer. *Phys. Chem. Chem. Phys.* **2011**, *13*, 9778−9788.
(17) Berhanu, W. M.; Hansmann, U. H. E. Side-chain Hydrophobicity and the Stability of Aβ_{16-22} Aggregates. *Protein Sci.* **2012**, *21*, 1837−1848.
(18) Li, Y.; Ji, C.; Xu, W.; Zhang, J. Z. Dynamical Stability and Assembly Cooperativity of β-Sheet Amyloid Oligomer- Effect of Polarization. *J. Phys. Chem. B* **2012**, *116*, 13368−13373.
(19) Matthes, D.; Gapsys, V.; Daebel, V.; de Groot, B. L. Mapping the Conformational Dynamics and Pathways of Spontaneous Steric Zipper Peptide Oligomerization. *PLoS ONE* **2011**, *6*, e19129.
(20) Berhanu, W. M.; Hansmann, U. H. E. Structure and Dynamics of Amyloid-β Segmental Polymorphisms. *PLoS ONE* **2012**, *7*, e41479.

(21) Viet, M. H.; Li, M. S. Amyloid Peptide Aβ40 Inhibits Aggregation of Aβ42: Evidence from Molecular Dynamics Simulations. *J. Chem. Phys.* **2012**, *136*, 245105.
(22) Liang, C.; Derreumaux, P.; Wei, G. Structure and Aggregation Mechanisms of Human beta2-microglobulin(83−99) Peptides Studied by Molecular Dynamics Simulations. *Biophys. J.* **2007**, *93*, 3353−3362.
(23) De Simone, A.; Derreumaux, P. Low Molecular Weight Oligomers of Amyloid Peptides Display β-barrel Conformations: A Replica Exchange Molecular Dynamics Study in Explicit Solvent. *J. Chem. Phys.* **2010**, *132*, 165103.
(24) Li, H.; Luo, Y.; Derreumaux, P.; Wei, G. Carbon Nanotube Inhibits the Formation of β-sheet-rich Oligomers of the Alzheimer's Amyloid $A\beta_{16-22}$ Peptide. *Biophys. J.* **2011**, *101*, 2267−76.
(25) Larini, L.; Shea, J. E. Role of β-Hairpin Formation in Aggregation: The Self-Assembly of the Amyloid-β(25−35) Peptide. *Biophys. J.* **2012**, *103*, 576−586.
(26) Matthes, D.; Gapsys, V.; de Groot, B. L. Driving Forces and Structural Determinants of Steric Zipper Peptide Oligomer Formation Elucidated by Atomistic Simulations. *J. Mol. Biol.* **2012**, *421*, 390−416.
(27) Piana, S.; Laio, A. A Bias-exchange Approach to Protein Folding. *J. Phys. Chem. B* **2007**, *111*, 4553−4559.
(28) Baftizadeh, F.; Biarnes, X.; Pietrucci, F.; Affinito, F.; Laio, A. A Multidimensional View of Amyloid Fibril Nucleation in Atomistic Detail. *J. Am. Chem. Soc.* **2012**, *134*, 3886.
(29) Gupta, P.; Hall, C. K.; Voegler, A. C. Effect of Denaturant and Protein Concentrations upon Protein Refolding and Aggregation: A Simple lattice Model. *Protein Sci.* **1998**, *7*, 2642−2652.
(30) Harrison, P. M.; Chan, H. S.; Prusiner, S. B.; Cohen, F. E. Conformational Propagation with Prion-like Characteristics in a Simple Model of Protein Folding. *Protein Sci.* **2001**, *10*, 819−835.
(31) Dima, R. I.; Thirumalai, D. Exploring Protein Aggregation and Self-propagation Using Lattice Models:Phase Diagram and Kinetics. *Protein Sci.* **2002**, *11*, 1036−1049.
(32) Li, M. S.; Klimov, D. K.; Straub, J. E.; Thirumalai, D. Probing the Mechanisms of Fibril Formation Using Lattice Models. *J. Chem. Phys.* **2008**, *129*, 175101.
(33) Nguyen, H. D.; Hall, C. K. Molecular Dynamics Simulations of Spontaneous Fibril Formation by Random-coil Peptides. *Proc. Natl. Acad. Sci. U.S.A.* **2004**, *101*, 16180−16185.
(34) Pellarin, R.; Caflisch, A. Interpreting the Aggregation Kinetics of Amyloid Peptides. *J. Mol. Biol.* **2006**, *360*, 882−892.
(35) Wei, G.; Mousseau, N.; Derreumaux, P. Computational Simulations of the Early Steps of Protein Aggregation. *Prion* **2007**, *1*, 3−8.
(36) Fawzi, N. L.; Kohlstedt, K. L.; Okabe, Y.; Head-Gordon, T. Protofibril Assemblies of the Arctic, Dutch, and Flemish Mutants of the Alzheimer's A-beta(1−40) Peptide. *Biophys. J.* **2008**, *94*, 2007−2016.
(37) Bellesia, G.; Shea, J. E. Diversity of Kinetic Pathways in Amyloid Fibril Formation. *J. Chem. Phys.* **2009**, *131*, 111102−1 − 111102−4.
(38) Urbanc, B.; Cruz, L.; Yun, S.; Buldyrev, S. V.; Bitan, G.; Teplow, D. B.; Stanley, H. E. *In silico* Study of Amyloid β-protein Folding and Oligomerization. *Proc. Natl. Acad. Sci. U.S.A.* **2004**, *101*, 17345−17350.
(39) Derreumaux, P.; Mousseau, N. Coarse-grained Protein Molecular Dynamics Simulations. *J. Chem. Phys.* **2007**, *126*, 025101−025106.
(40) Sorensen, J.; Periole, X.; Skeby, K. K.; Marrink, S. J.; Schiott, B. Protofibrillar Assembly Toward the Formation of Amyloid Fibrils. *Phys. Chem. Lett.* **2012**, *2*, 2385−2390.
(41) Li, D. W.; Mohanty, S.; Irback, A.; Huo, S. Formation and Growth of Oligomers: A Monte Carlo Study of an Amyloid Tau Fragment. *PLoS Comput. Biol.* **2008**, *4*, e1000238.
(42) Nasica-Labouze, J.; Meli, M.; Derreumaux, P.; Colombo, G.; Mousseau, N. A Multiscale Approach to Characterize the Early Aggregation Steps of the Amyloid-forming Peptide GNNQQNY from the Yeast Prion sup-35. *PLoS Comput. Biol.* **2011**, *7*, 1002051.
(43) Chebaro, Y.; Derreumaux, P. Targeting the Early Steps of $A\beta_{16-22}$ Protofibril Disassembly by N-methylated Inhibitors: A Numerical Study. *Proteins* **2009**, *75*, 442−452.
(44) Bieler, N. S.; Knowles, T. P. J.; Frenkel, D.; Vacha, R. Connecting Macroscopic Observables and Microscopic Assembly Events in Amyloid Formation Using Coarse Grained Simulations. *PLoS Comput. Biol.* **2012**, *8*, e1002692.
(45) Melquiond, A.; Mousseau, N.; Derreumaux, P. Structures of Soluble Amyloid Oligomers From Computer Simulation. *Proteins* **2006**, *65*, 180−191.
(46) Lu, Y.; Derreumaux, P.; Guo, Z.; Mousseau, N.; Wei, G. Thermodynamics and Dynamics of Amyloid Peptide Oligomerization are Sequence Dependent. *Proteins* **2009**, *75*, 954−963.
(47) Santini, S.; Wei, G.; Mousseau, N.; Derreumaux, P. Pathway Complexity of Alzheimer's beta-amyloid $A\beta_{16-22}$ Peptide Assembly. *Structure* **2004**, *12*, 1245−1255.
(48) Santini, S.; Mousseau, N.; Derreumaux, P. In Silico Assembly of Alzheimer's $A\beta_{16-22}$ Peptide into β-sheets. *J. Am. Chem. Soc.* **2004**, *126*, 11509−11516.
(49) Melquiond, A.; Boucher, G.; Mousseau, N.; Derreumaux, P. Following the Aggregation of Amyloid-forming Peptides by Computer Simulations. *J. Chem. Phys.* **2005**, *122*, 174904.
(50) Song, W.; Wei, G.; Mousseau, N.; Derreumaux, P. Self-assembly of the beta 2-microglobulin NHVTLSQ Peptide Using a Coarse-grained Protein Model Reveals β-barrel Species. *J. Phys. Chem. B* **2008**, *112*, 4410−4418.
(51) Sawaya, M. R.; Sambashivan, S.; Nelson, R.; Ivanova, M. I.; Sievers, S. A.; Apostol, M. I.; Thompson, M. J.; Balbirnie, M.; Wiltzius, J. J. W.; McFarlane, H. T.; et al. Atomic Structures of Amyloid Cross-β Spines Reveal Varied Steric Zippers. *Nature* **2005**, *447*, 453−457.
(52) Reddy, G.; Straub, J. E.; Thirumalai, D. Dry Amyloid Fibril Assembly in a yeast Prion Peptide is Mediated by Long-lived Structures Containing Water Wires. *Proc. Natl. Acad. Sci. U.S.A.* **2010**, *107*, 21459−21464.
(53) Tirado-Rives, J.; Jorgensen, W. L. Molecular-dynamics Simulations of the Unfolding of an Alpha-helical Analog of Ribonuclease-A S-peptide in Water. *Biochemistry* **1991**, *30*, 3864−3871.
(54) MacKerell, J. A.; Bashford, D.; Bellott, M.; Dunbrack, R. L.; Evanseck, J. D.; Field, M. J.; Fischer, S.; Gao, J.; Guo, H.; Ha, S.; et al. All-atom Empirical Potential for Molecular Modeling and Dynamics Studies of Proteins. *J. Phys. Chem. B* **1998**, *102*, 3586−3616.
(55) Berendsen, H. J. C.; Postma, J. P. M.; van Gunsteren, W. F.; Dinola, A.; Haak, J. R. Molecular Dynamics With Coupling to an External Bath. *J. Chem. Phys.* **1984**, *81*, 3684−3690.
(56) Lindahl, E.; Hess, B.; van der Spoel, D. GROMACS 3.0: A Package for Molecular Simulation and Trajectory Analysis. *J. Mol. Mod.* **2001**, *7*, 306−317.
(57) Ryckaert, J. P.; Cicotti, G.; Berendsen, H. J. C. Numerical Integration of the Cartesian Equations of Motion of a System with Constraints: Molecular Dynamics of n-Alkanes. *J. Comput. Phys.* **1977**, *23*, 327−341.
(58) Darden, T.; York, D.; Pedersen, L. Particle Mesh Ewald: An Nlog(N) Method for Ewald Sums in Large Systems. *J. Chem. Phys.* **1993**, *98*, 10089−10092.
(59) Patriksson, A.; van der Spoel, D. A Temperature Predictor for Parallel Tempering Simulations. *Phys. Chem. Chem. Phys.* **2008**, *10*, 2073−2077.
(60) http://folding.bmc.uu.se/remd/index.php.
(61) Klimov, D. K.; Thirumalai, D. Dissecting the Assembly of $A\beta_{16-22}$ Amyloid Peptides into Antiparallel β sheets. *Structure* **2003**, *11*, 295−307.
(62) Frishman, D.; Argos, P. Knowledge-Based Protein Secondary Structure Assignment Proteins. *Proteins* **1995**, *23*, 566−579.
(63) Zannoni, C. *Advances in the Computer Simulations of Liquid Crystals*; Kluwer Academics: Dordrecht, 2000.
(64) Nguyen, P.; Li, M. S.; Stock, G.; Staub, J. E.; Thirumalai, D. Monomer Adds to Preformed Structured Oligomers of Aβ-peptides by a Two-stage Dock-lock Mechanism. *Proc. Natl. Acad. Sci. U.S.A.* **2007**, *104*, 111−116.
(65) Serio, T. R.; Cashikar, A. G.; Kowal, A. S.; Sawicki, G. J.; Moslehi, J. J.; Serpell, L.; Arnsdorf, M. F.; Lindquist, S. L. Nucleated

Conformational Conversion and the Replication of Conformational Information by a Prion Determinant. *Science* **2000**, *25*, 1317−1321.
(66) Cheon, M.; Chang, I.; Mohanty, S.; Luheshi, L. M.; Dobson, C. M.; Vendruscolo, M.; Favrin, G. Structural Reorganisation and Potential Toxicity of Oligomeric Species Formed during the Assembly of Amyloid Fibrils. *PLoS Comput. Biol.* **2007**, *3*, e173.
(67) Nasica-Labouze, J.; Mousseau, N. Kinetics of Amyloid Aggregation: A Study of the GNNQQNY Prion Sequence. *PLoS Comput. Biol.* **2012**, *8*, 1002782.
(68) Wei, G.; Mousseau, N.; Derreumaux, P. Sampling the Self-assembly Pathways of KFFE Hexamers. *Biophys. J.* **2004**, *87*, 3648−3656.
(69) Cheon, M.; Chang, I.; Hall, C. K. Spontaneous Formation of Twisted Aβ_{16-22} Fibrils in Large-scale Molecular-dynamics Simulations. *Biophys. J.* **2011**, *101*, 2493−2501.
(70) Bellesia, G.; Shea, J. E. What Determines the Structure and Stability of KFFE Monomers, Dimers, and Protofibrils? *Biophys. J.* **2009**, *96*, 875−886.
(71) Lu, Y.; Wei, G.; Derreumaux, P. Structural, Thermodynamical, and Dynamical Properties of Oligomers Formed by the Amyloid NNQQ Peptide: Insights from Coarse-grained Simulations. *J. Chem. Phys.* **2012**, *137*, 025101.
(72) Wagoner, V. A.; Cheon, M.; Chang, I.; Hall, C. K. Fibrillization Propensity for Short Designed Hexapeptides Predicted by Computer Simulation. *J. Mol. Biol.* **2012**, *416*, 598−609.
(73) Cheon, M.; Chang, I.; Hall, C. K. Influence of Temperature on Formation of Perfect tau Fragment Fibrils Using PRIME20/DMD Simulations. *Protein Sci.* **2012**, *21*, 1514−1527.
(74) Wu, C.; Hei, H. X.; Duan, Y. Elongation of Ordered Peptide Aggregate of an Amyloidogenic Hexapeptide (NFGAIL) Observed in Molecular Dynamics Simulations with Explicit Solvent. *J. Am. Chem. Soc.* **2005**, *127*, 13530−13537.
(75) Auer, S.; Ricchiuto, P.; Kashchiev, D. Two-step Nucleation of Amyloid Fibrils: Omnipresent or Not? *J. Mol. Biol.* **2012**, *422*, 723−730.
(76) Knowles, T. P. J.; Waudby, C. A.; Devlin, G. L.; Cohen, S. I. A.; Aguzzi, A.; Vendruscolo, M.; Terentjev, E. M.; Welland, M. E.; Dobson, C. M. An Analytical Solution to the Kinetics of Breakable Filament Assembly. *Science* **2009**, *326*, 1533−1537.
(77) Pellarin, R.; Schuetz, P.; Guarnera, E.; Caflisch, A. Amyloid Fibril Polymorphism is Under Kinetic Control. *J. Am. Chem. Soc.* **2009**, *132*, 14960−14970.
(78) Hills, R. D.; Brooks-III, C. L. Hydrophobic Cooperativity as a Mechanism for Amyloid Nucleation. *J. Mol. Biol.* **2007**, *368*, 894−901.
(79) Rohrig, U. F.; Laio, A.; Tantalo, N.; Parrinello, M.; Petronzio, R. Stability and Structure of Oligomers of the Alzheimer Peptide Aβ_{16-22}: From the Dimer to the 32-mer. *Biophys. J.* **2005**, *91*, 3217−3229.
(80) Co, N. T.; Li, M. S. New Method for Determining Size of Critical Nucleus of Fibril Formation of Polypeptide Chains. *J. Chem. Phys.* **2007**, *137*, 095101.
(81) Qiang, W. Q. Q.; Yau, W. M.; Tycko, R. Structural Evolution of Iowa Mutant beta-amyloid Fibrils from Polymorphic to Homogeneous States under Repeated Seeded Growth. *J. Am. Chem. Soc.* **2011**, *133*, 4018−4029.
(82) Colletier, J. P.; Laganowsky, A.; Landau, M.; Zhao, M.; Soriaga, A. B.; Goldschmidt, L.; Flot, D.; Cascio, D.; Sawaya, M. R.; Eisenberg, D. Molecular Basis for Amyloid-β Polymorphism. *Proc. Natl. Acad. Sci. U.S.A.* **2011**, *108*, 16938−16943.
(83) Lansbury, P. T.; Costa, P. R.; Griffiths, J. M.; Simon, E. J.; Auger, M.; Halverson, K. J.; Kocisko, D. A.; Hendsch, Z. S.; Ashburn, T. T.; Spencer, R. G.; et al. Structural Model for the beta-amyloid Fibril Based on Interstrand Alignment of an Antiparallel-sheet Comprising a C-terminal Peptide. *Nat. Struct. Mol. Biol.* **1995**, *2*, 990−998.